Fuzzy Sliding Mode Control of an Upper Limb Exoskeleton for Robot-assisted Rehabilitation

Qingcong Wu, Xingsong Wang, Fengpo Du, Qing Zhu
School of Mechanical Engineering, Southeast University
Nanjing, China
E-mail: xswang@seu.edu.cn

***Abstract*—Robot-assisted therapy has become an important technology used to restore and reinforce the motor functions of the patients with neuromuscular disorders. In this paper, we proposed an upper-limb exoskeleton intended to assist the rehabilitation training of shoulder, elbow and wrist. The proposed therapeutic exoskeleton has an anthropomorphic structure able to match the upper-limb anatomy and enable natural human-robot interaction. A modified sliding mode control (SMC) strategy consisting of a proportional-integral-derivative (PID) sliding surface and a fuzzy hitting control law is developed to guarantee robust tracking performance and reduce the chattering effect. The Lyapunov theorem is utilized to demonstrate the system stability. In order to evaluate the effectiveness of proposed algorithm, several trajectory tracking experiments were conducted based on a real-time control system. Experimental results are presented to prove that, when compared to the conventional PID controller, the fuzzy SMC strategy can effectively reduce the tracking errors and achieve favorable control performance.**

Keywords—upper-limb exoskeleton; rehabilitation; sliding mode control; PID sliding surface; fuzzy hitting control law

I. INTRODUCTION

Robotic system has great application value in neural rehabilitation. According to the statistical data of the World Health Organization (WHO), nowadays there are more than 15 million people suffering from the effects of stroke and spinal cord injury (SCI) in the world. Stroke is a highly prevalent disease leading to neurologic impairments and movement disorders. Studies in clinical robot-assisted rehabilitation have proved that therapeutic robot systems can provide effective assistance with various kinds of training modes to the patients. In addition, it allows the therapists to monitor the rehabilitation progress and adjust the training plans reasonably. The existing therapeutic devices can be distinguished into two categories: end-effectors-based robots and wearable exoskeletons. In the first case, the robot is connected with the patient's hand at one point [1-2]. In the second case, the exoskeleton is attached to several points of upper limb and required to imitate human anatomy [3-5].

For the motivation of developing therapeutic robot systems, the controller design is a significant challenge in providing high-quality treatments and services. In recent years, widespread researches have been focused on developing different control strategies for rehabilitation training. The control algorithms for the end-effector-based robots and exoskeletons are quite complex due to the nonlinear properties of kinematic and kinetic models. Ju *et al.* [6] developed a five-bar-link robot arm and a novel hybrid position/force controller incorporating fuzzy logic for the rehabilitation of shoulder and elbow. Tobias *et al.* [7] proposed a hybrid PD/impedance control approach for the disable patients to conduct labyrinth game therapy based on the ARMin exoskeleton. A pneumatic-muscle-driven upper limb rehabilitation robot was developed by Jiang *et al.* [8]. Besides, a neuron PI controller combined with feedforward control was proposed for position control of the robotic joints. Wen *et al.* [9] developed a model-free PID type admittance controller, whose parameters can be modulated according to human impedance characteristics, for the exoskeleton system named EXO-UL7.

The sliding mode control (SMC) is an effective nonlinear robust strategy which can theoretically ensure trajectory tracking performance in the presence of system perturbation, external disturbance, and parametric uncertainties. The SMC strategy has been successfully applied in various robotic motion control systems, such as robot manipulator [10], mobile robot [11], induction motor control [12], rehabilitation robot [13], shape memory alloy actuator [14], and high-speed linear axis actuation [15]. However, the discontinuous nature of SMC introduces many drawbacks in practical application, such as high frequency output oscillations, i.e. chattering, and unnecessarily large control signals to overcome the model uncertainties [16]. The chattering phenomenon can excite high-frequency plant dynamics and, as a result, lead to unforeseen instabilities. To overcome these problems, several strategies of chattering reduction have been proposed. Rahman *et al.* [17] improve the original switching control law of SMC by replacing the signum function with a saturation function. Bartolini *et al.* [18] developed a second-order SMC algorithm, without observers and differential inequalities, to solve the chattering elimination problem.

The main purpose of this paper is to present an upper-limb exoskeleton with nine degrees of motion (DOFs) for robot-assisted rehabilitation of shoulder, elbow and wrist. This therapeutic robot system is developed from our previous active gravity balanced exoskeleton [19]. The major mechanical structure and the real-time control system are described. A modified SMC algorithm with a PID sliding surface is developed to guarantee robust tracking performance. Besides,

978-1-4799-6477-2/15/$31.00 ©2015 IEEE

for the purpose of minimizing the chattering problem, a fuzzy logic controller is proposed to optimize the hitting control law. The convergence of the closed-loop system is demonstrated by using Lyapunov stability theory. Finally, trajectories tracking experiments with fuzzy SMC algorithm and normal PID control law are carried out respectively to compare the tracking performance and verify the effectiveness of the proposed strategy. The experimental results are reported and discussed.

II. Design of The Rehabilitation Exoskeleton

A. Mechanical design

The mechanical structure of the proposed exoskeleton is designed to be isomorphic to the upper limb of human, as shown in Fig. 1. The rehabilitative device has three active DOFs to perform spatial shoulder movements, i.e. internal/external, abduction/adduction, and flexion/extension, two active DOFs at the elbow to enable flexion/extension and pronation/supination movements, and two active DOFs at the wrist to enable flexion/extension and ulnal/radial deviation movements. In addition, since the rotation center of glenohumeral joint shifts according to shoulder girdle movements, the exoskeleton is mounted on a mobile platform with two passive DOFs to compensate the misalignment generated in horizontal plane. The shoulder joint and the elbow joint of exoskeleton system are actuated by AC servo motors (YASKAWA-SGMAV 04AA41, reduction ratio-40:1) via Bowden-cable transmission system. The detail description of the Bowden-cable actuation has been proposed in our previous research [20-21]. The wrist joint is directly driven by two high precision brushless DC motor (ASLONG-JGA25). The joint positions are measured with conductive plastic angle potentiometer (WDJ22A-10K). In order to incorporate the human-robot interaction into rehabilitation treatment, a force/torque sensor (NANO-25-ATI) is mounted at the end-effector to measure the interactive force. The exoskeleton is kept in gravity balanced state by utilizing auxiliary links and zero free-length springs to balance the gravity and maintain the potential energy invariant with all configurations [19]. The operational security can be guaranteed by mounting mechanical end stoppers on robot joints to avoid excessive rotation and extension. In addition, the patient and therapist are all required to hold a dead-man button which can shut down the robotic system in emergency situation.

B. Control system

A real-time control system has been developed based on the MATLAB/RTW environment and used for the training control of the rehabilitation robot. The major hardware architecture of the proposed control system is presented in Fig. 2. There are two industrial computers (IPC-610H, Advantech Inc.) working as the host computer and the real-time target, respectively. The host computer makes use of MATLAB/Simulink to specify the control algorithms, and Real-Time Workshop to generate the corresponding downloadable C code. And then the target computer downloads and runs the generated code and, finally, sends the appropriate commands to the motor servo drivers with a sampling time of 1ms. Communication between the host computer and the target computer is supported via a serial

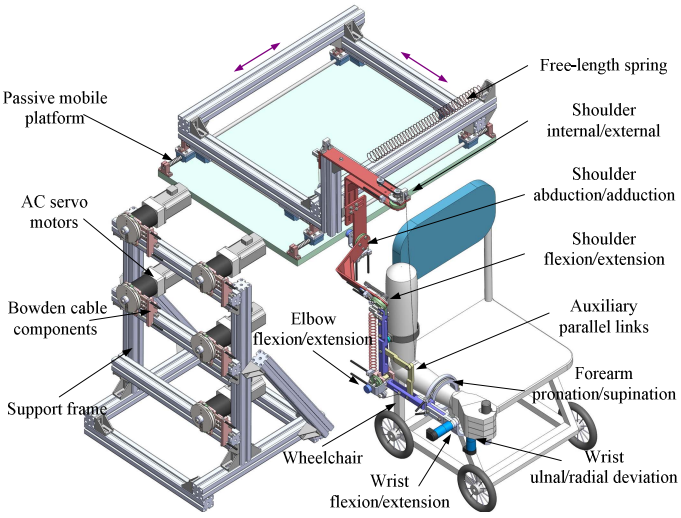

Fig. 1. Mechanical structure of the upper-limb rehabilitation exoskeleton.

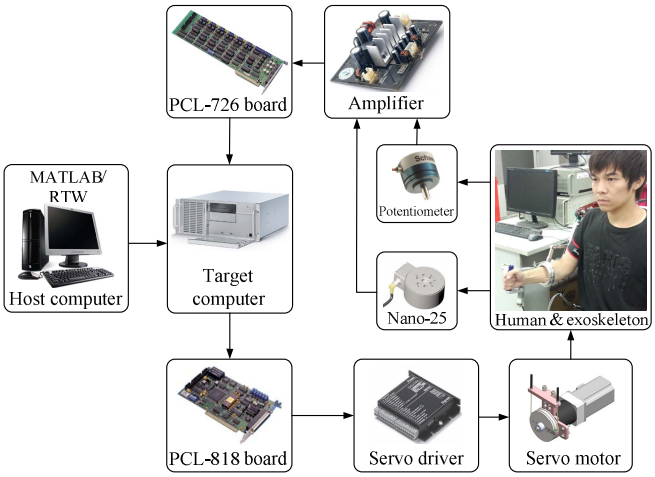

Fig. 2. Hardware architecture of the control system

cable. The practical feedback signals measured from the potentiometers and force/torque sensor are amplified by a transistor made power amplifier and acquired via an A/D data acquisition card (PCL-818, Advantech Inc.). The generated commands from the target computer are transformed into analog output signals via a D/A card (PCL-726, Advantech Inc.).

III. Development of Fuzzy Sliding Mode Control

A. Dynamic modeling

Using Lagrange methodology, the robotic dynamics of the upper-limb exoskeleton combined with the subject's limb can be described as the following nonlinear differential equation:

$$\mathbf{M}(\boldsymbol{\theta})\ddot{\boldsymbol{\theta}} + \mathbf{V}(\boldsymbol{\theta},\dot{\boldsymbol{\theta}}) + \mathbf{G}(\boldsymbol{\theta}) + \mathbf{F}(\boldsymbol{\theta},\dot{\boldsymbol{\theta}}) = \boldsymbol{\tau} \qquad (1)$$

where $\boldsymbol{\theta}, \dot{\boldsymbol{\theta}}, \text{and } \ddot{\boldsymbol{\theta}} \in R^7$ denote the joint positions, velocities, and accelerations vector respectively; $\boldsymbol{\tau} \in R^7$ is the driving torques vector; $\mathbf{M}(\boldsymbol{\theta}) \in R^{7\times 7}$ is the inertia matrix; $\mathbf{V}(\boldsymbol{\theta},\dot{\boldsymbol{\theta}}) \in R^7$ represents the vector of Coriolis and centrifugal torques; $\mathbf{G}(\boldsymbol{\theta}) \in R^7$

denotes the vector of gravitational torques; $\mathbf{F}(\boldsymbol{\theta},\dot{\boldsymbol{\theta}}) \in R^7$ is the friction vector. Since the upper-limb exoskeleton system is kept in the static balanced state during operation [19], the gravity vector of the dynamic model can be eliminated. Therefore, (1) can be rewritten as:

$$\mathbf{M}(\boldsymbol{\theta})\ddot{\boldsymbol{\theta}} + \mathbf{V}(\boldsymbol{\theta},\dot{\boldsymbol{\theta}}) + \mathbf{F}(\boldsymbol{\theta},\dot{\boldsymbol{\theta}}) = \boldsymbol{\tau} \tag{2}$$

Note that the friction vector is modeled as a Coulomb+viscous friction model, which can be expressed as:

$$F_i(\theta,\dot{\theta}) = \begin{cases} b_i\dot{\theta}_i + \tau_{ci} & \text{when } \dot{\theta}_i > 0 \\ b_i\dot{\theta}_i - \tau_{ci} & \text{when } \dot{\theta}_i < 0, \quad i = 1,2,\cdots,7 \end{cases} \tag{3}$$

where b_i represents the viscous coefficient; τ_{ci} denotes the Coulomb friction torque; b_i and τ_{ci} can be determined empirically.

Since the $\mathbf{M}(\boldsymbol{\theta})$ matrix is symmetrical and positive definite, (2) can be converted into (4) to express the accelerations vector:

$$\ddot{\boldsymbol{\theta}} = \mathbf{M}(\boldsymbol{\theta})^{-1}\left[\boldsymbol{\tau} - \mathbf{V}(\boldsymbol{\theta},\dot{\boldsymbol{\theta}}) - \mathbf{F}(\boldsymbol{\theta},\dot{\boldsymbol{\theta}})\right] \tag{4}$$

The position tracking error of the closed-loop system is defined as:

$$\mathbf{e}(t) = \boldsymbol{\theta}_\mathbf{d}(t) - \boldsymbol{\theta}(t) \tag{5}$$

where $\mathbf{e}(t) \in R^7$ is tracking error vector, $\boldsymbol{\theta}_\mathbf{d}(t) \in R^7$ is the reference trajectory.

B. Sliding model controller

A sliding model controller with a PID sliding surface is developed to enforce the tracking error to approach to the sliding surface and ensure expected control performance and specifications. The switching function of the sliding surface is defined in the tracking error state and expressed as:

$$\mathbf{s}(t) = \mathbf{K}_\mathbf{p}\mathbf{e}(t) + \mathbf{K}_\mathbf{i}\int \mathbf{e}(\xi)d\xi + \mathbf{K}_\mathbf{d}\frac{d}{dt}\mathbf{e}(t) \tag{6}$$

Here $\mathbf{s}(t) \in R^7$ represents the sliding variable vector; $\mathbf{K}_\mathbf{p}, \mathbf{K}_\mathbf{i}, \text{and } \mathbf{K}_\mathbf{d} \in R^{7\times 7}$ are the positive diagonal matrixes of proportional gain, integral gain, and derivative gain.

The expression for the deviation of the sliding variable is:

$$\dot{\mathbf{s}}(t) = \mathbf{K}_\mathbf{p}\dot{\mathbf{e}}(t) + \mathbf{K}_\mathbf{i}\mathbf{e}(t) + \mathbf{K}_\mathbf{d}\ddot{\mathbf{e}}(t) \tag{7}$$

then, inserting (4) and (5) into (7), the following equation is obtained:

$$\begin{aligned} \dot{\mathbf{s}}(t) &= \mathbf{K}_\mathbf{p}\dot{\mathbf{e}}(t) + \mathbf{K}_\mathbf{i}\mathbf{e}(t) + \mathbf{K}_\mathbf{d}\left(\ddot{\boldsymbol{\theta}}_\mathbf{d} - \ddot{\boldsymbol{\theta}}\right) \\ &= \mathbf{K}_\mathbf{p}\dot{\mathbf{e}}(t) + \mathbf{K}_\mathbf{i}\mathbf{e}(t) + \mathbf{K}_\mathbf{d}\ddot{\boldsymbol{\theta}}_\mathbf{d} - \mathbf{K}_\mathbf{d}\mathbf{M}(\boldsymbol{\theta})^{-1}\left[\boldsymbol{\tau} - \mathbf{V}(\boldsymbol{\theta},\dot{\boldsymbol{\theta}}) - \mathbf{F}(\boldsymbol{\theta},\dot{\boldsymbol{\theta}})\right] \\ &= \mathbf{K}_\mathbf{p}\dot{\mathbf{e}}(t) + \mathbf{K}_\mathbf{i}\mathbf{e}(t) + \mathbf{K}_\mathbf{d}\ddot{\boldsymbol{\theta}}_\mathbf{d} - \mathbf{K}_\mathbf{d}\mathbf{M}(\boldsymbol{\theta})^{-1}\boldsymbol{\tau} + \mathbf{K}_\mathbf{d}\mathbf{M}(\boldsymbol{\theta})^{-1}\mathbf{V}(\boldsymbol{\theta},\dot{\boldsymbol{\theta}}) \\ &\quad + \mathbf{K}_\mathbf{d}\mathbf{M}(\boldsymbol{\theta})^{-1}\mathbf{F}(\boldsymbol{\theta},\dot{\boldsymbol{\theta}}) \end{aligned} \tag{8}$$

In the design of SMC system, the control input $\mathbf{u}$ is composed by an equivalent control term $\mathbf{u}_{\mathbf{eq}}$ and a hitting control term $\mathbf{u}_{\mathbf{disc}}$ [22]. Totally, the SMC law is described as:

$$\mathbf{u} = \mathbf{u}_{\mathbf{eq}} + \mathbf{u}_{\mathbf{hit}} \tag{9}$$

Here, the equivalent control term carries the system state vector over the reference trajectory and, moreover, determines the dynamics of the system on the sliding surface [23]. $\mathbf{u}_{\mathbf{eq}}$ can be derived by recognizing

$$\dot{\mathbf{s}}(t) = 0 \tag{10}$$

Substituting (8) into (10), we can get

$$\mathbf{u}_{\mathbf{eq}} = \boldsymbol{\tau} = \mathbf{M}(\boldsymbol{\theta})\left[\mathbf{K}_\mathbf{d}^{-1}\mathbf{K}_\mathbf{p}\dot{\mathbf{e}}(t) + \mathbf{K}_\mathbf{d}^{-1}\mathbf{K}_\mathbf{i}\mathbf{e}(t) + \ddot{\boldsymbol{\theta}}_\mathbf{d}\right] + \mathbf{V}(\boldsymbol{\theta},\dot{\boldsymbol{\theta}}) + \mathbf{F}(\boldsymbol{\theta},\dot{\boldsymbol{\theta}}) \tag{11}$$

The hitting control term is used to eliminate the effect of the undesirable perturbations and keep the system state vector to the reference trajectory. $\mathbf{u}_{\mathbf{hit}}$ is described as follow:

$$\mathbf{u}_{\mathbf{hit}} = \varepsilon\mathbf{M}(\boldsymbol{\theta})\mathbf{K}_\mathbf{d}^{-1}\text{sat}(\mathbf{s}) \tag{12}$$

$$\text{sat}(\mathbf{s}) = \begin{cases} \dfrac{\mathbf{s}}{\delta} & \text{when } |\mathbf{s}| < \delta \\ \text{sign}(\mathbf{s}) & \text{when } |\mathbf{s}| > \delta \end{cases} \tag{13}$$

where ε is the positive output gain of the hitting controller; δ is a positive constant representing the boundary layer thickness of the saturation function.

The Lyapunov stability theory is used to demonstrate the system stability with the proposed SMC scheme. Let the Lyapunov function candidate chosen as

$$\mathbf{V} = \frac{1}{2}\mathbf{s}^\mathrm{T}(t)\mathbf{s}(t) \tag{14}$$

Differentiating $\mathbf{V}$ with respect to t and combining (8)~(13), we can get

$$\begin{aligned} \dot{\mathbf{V}} &= \mathbf{s}^\mathrm{T}(t)\dot{\mathbf{s}}(t) \\ &= \mathbf{s}^\mathrm{T}(t)\mathbf{K}_\mathbf{p}\dot{\mathbf{e}}(t) + \mathbf{K}_\mathbf{i}\mathbf{e}(t) + \mathbf{K}_\mathbf{d}\ddot{\boldsymbol{\theta}}_\mathbf{d} - \mathbf{K}_\mathbf{d}\mathbf{M}(\boldsymbol{\theta})^{-1}(\mathbf{u}_{\mathbf{eq}} + \mathbf{u}_{\mathbf{hit}}) \\ &\quad + \mathbf{K}_\mathbf{d}\mathbf{M}(\boldsymbol{\theta})^{-1}\mathbf{V}(\boldsymbol{\theta},\dot{\boldsymbol{\theta}}) + \mathbf{K}_\mathbf{d}\mathbf{M}(\boldsymbol{\theta})^{-1}\mathbf{F}(\boldsymbol{\theta},\dot{\boldsymbol{\theta}}) \\ &= -\varepsilon\mathbf{s}^\mathrm{T}\text{sat}(\mathbf{s}) \end{aligned} \tag{15}$$

Now, inserting (13) into (15) yields

$$\begin{aligned} \dot{\mathbf{V}} &= -\varepsilon\mathbf{s}^\mathrm{T}\text{sat}(\mathbf{s}) \\ &= \begin{cases} \dfrac{-\varepsilon\mathbf{s}^\mathrm{T}\mathbf{s}}{\delta} < 0 & \text{when } |\mathbf{s}| < \delta \\ -\varepsilon\sum_{i=1}^{7}|s_i| < 0 & \text{when } |\mathbf{s}| > \delta \end{cases} \end{aligned} \tag{16}$$

Here, it should be noted that $\mathbf{V}$ is positive definite and, meanwhile, $\dot{\mathbf{V}}$ is negative definite. Therefore, the control system is asymptotically stable and the tracking error converges to the sliding surface $\dot{\mathbf{s}}(t) = 0$.

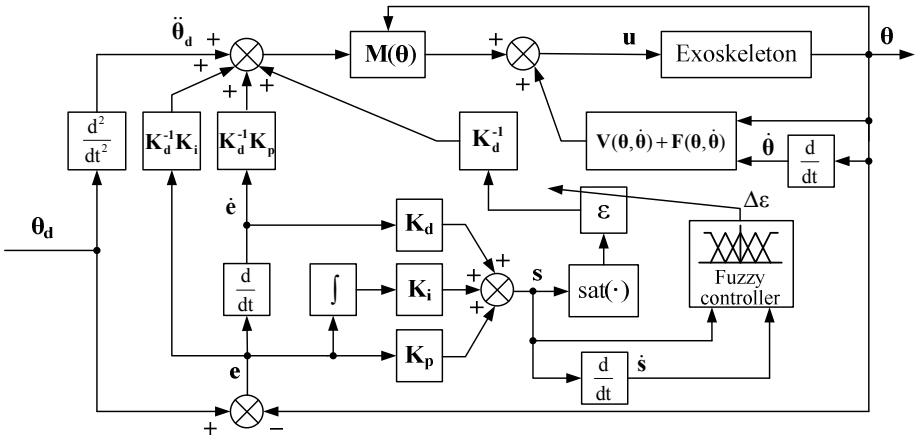

Fig. 3. The block diagram of the fuzzy sliding mode control scheme

C. *Fuzzy system in adjusting SMC parameter*

The SMC algorithm could introduce undesirable chattering problem to the exoskeleton, since the saturation function of the hitting term control law shown in (12) and (13) is unsmooth when the system cross the sliding surface. The high-frequency oscillations are directly defined by the output gain of the hitting controller, i.e. ε. Therefore, in order to reduce the chattering level and, at the same time, the required time for the tracking error to reach the sliding surface, a nonlinear fuzzy function of $\mathbf{s}(t)$ and $\dot{\mathbf{s}}(t)$ is developed to adjust the value of ε. The expression of ε can be written as:

$$\varepsilon=\hat{\varepsilon}+\Delta\varepsilon \tag{17}$$

$$\Delta\varepsilon = \mathrm{FC}\left(\mathbf{s}(t),\dot{\mathbf{s}}(t)\right)$$

where $\hat{\varepsilon}$ represents the original output gain of the hitting controller; $\Delta\varepsilon$ denotes the adjusted value of ε determined by the fuzzy controller $\mathrm{FC}\left(\mathbf{s}(t),\dot{\mathbf{s}}(t)\right)$. When $\mathbf{s}^{\mathrm{T}}(t)\dot{\mathbf{s}}(t)>0$, the sliding variable tends to move away from the sliding surface. For bigger $|\mathbf{s}|$ or $|\dot{\mathbf{s}}|$, ε should be increased to enforce the sliding variable to return to the sliding surface and reduce the reaching time. On the contrary, when $\mathbf{s}^{\mathrm{T}}(t)\dot{\mathbf{s}}(t)<0$, the sliding variable tends to approach to the sliding surface. For smaller $|\mathbf{s}|$ or bigger $|\dot{\mathbf{s}}|$, ε should be decreased to minimize the chattering level. The completed block diagram of the fuzzy sliding mode control scheme is represented in Fig. 3.

The fuzzy controller is established based on the Mamdani model and applied to the SMC system for online turning of ε. The fuzzy turning rules are represented in Table. I, with $\mathbf{s}(t)$ and $\dot{\mathbf{s}}(t)$ as the input linguistic variables and $\Delta\varepsilon$ as the output linguistic variable. Each input rule combination activates one output action. The characters NL, NM, ZE, PS, PM, PB, and PL denotes negative large, negative medium, zero, positive small, positive medium, positive big, and positive large, respectively. Triangle-shape and trapezoid-shape membership functions are applied for the inputs and outputs of the fuzzy logic, as shown in Figs. 4~6. The membership functions are defuzzified by using the center of gravity (COG) method as follow:

TABLE I. THE FUZZY CONTROL RULES FOR $\Delta\varepsilon$

$\mathbf{s}(t)$	$\dot{\mathbf{s}}(t)$				
	NL	NM	ZE	PM	PL
NL	PL	PL	PB	PM	PM
NM	PB	PB	PM	PS	PS
ZE	ZE	ZE	ZE	ZE	PS
PM	ZE	PS	PS	PM	PB
PL	PS	PS	PM	PB	PL

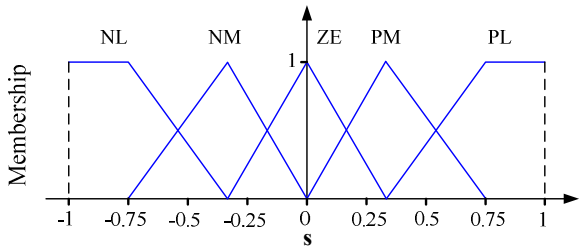

Fig. 4. The input membership function for $\mathbf{s}(t)$

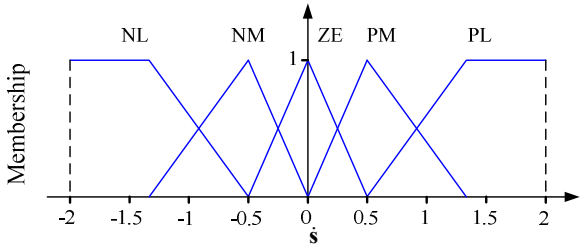

Fig. 5. The input membership function for $\dot{\mathbf{s}}(t)$

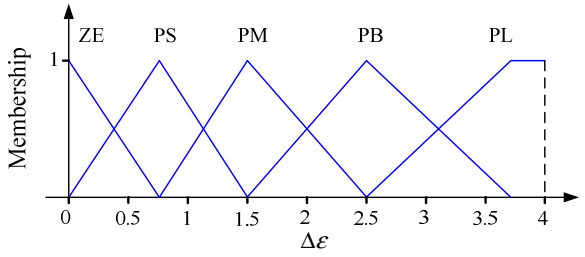

Fig. 6. The output membership function for $\Delta\varepsilon$

$$\Delta\varepsilon = \frac{\sum_{j=1}^{n} u_j A(u_j)}{\sum_{j=1}^{n} A(u_j)} \tag{18}$$

where $\Delta\varepsilon$ is the output of fuzzy control; n represents the number of the output quantization levels; $A(u_j)$ denotes the firing strength of the inferred fuzzy set corresponding to the support value u_j, which can be obtained using the Zadeh fuzzy synthesis method

$$A(u) = \bigcup_{i=1}^{m} \lambda_i A_i(u) \tag{19}$$

$$\lambda_i = \min\left\{ P_1^i\left(\frac{\mathbf{s}(t)}{dt}\right), P_2^i\left(\frac{\dot{\mathbf{s}}(t)}{dt}\right)\right\} \tag{20}$$

Here λ_i represents the weight of the i th fuzzy control rule; m denotes the total rules number; A_i is the output fuzzy set of the i th rule; P_1^i and P_2^i denote the input fuzzy sets of $\mathbf{s}(t)$ and $\dot{\mathbf{s}}(t)$.

IV. Experiments and Results

In order to evaluate the performance of the proposed fuzzy SMC algorithm presented in the previous section, preliminary trajectory tracking experiments were carried out with a subject (weight: 60 kg; height: 1.7 m) passively wearing the exoskeleton, as shown in Fig. 7. The subject was required to remain totally relaxed and not produce any muscular activation to the exoskeleton during operation. This means that the exoskeleton apply all the necessary driving torques to perform the training exercise. The passive movement therapy is usually applied to the impaired patients in the initial stage of the rehabilitation to prevent muscle atrophy and joint spasticity.

The tracking experiments were conducted on the internal/external rotation DOF of shoulder. Tracking performances of fuzzy SMC were compared to that of the conventional PID controller. During the comparative experiments, the servo motor used for the actuation of shoulder internal/external movement was run in torque control mode to output expected driving torque. Meanwhile, the other servo motors were all run in position control mode to keep the corresponding robotic joint motionless. The dynamic parameters of the exoskeleton and human upper limb can be obtained according to the developed virtual prototype model and the anthropometry in movement biomechanics [24]. The gain coefficients of the conventional PID controller, which were firstly estimated using the Ziegler-Nichols method [25] and then carefully turned by trial and error, were set to P=8.5, I=3.8, and D=1.2 as the as proportional, integral, and derivative respectively. On the other hand, the parameters of the PID sliding surface of the shoulder internal/external joint were set to k_{p1}=4.2, k_{i1}=2.4, and k_{d1}=0.8. The original output gain of the hitting controller was selected to be $\hat{\varepsilon}$ =3.

The proposed comparative position tracking tests were conducted with a fifteen-seconds-long sinusoid wave trajectory. The rehabilitation movement started with a frequency of 0.25 Hz and amplitude of 45 degrees for the first eight seconds, and then changed to 0.5 Hz and 60 degrees for the next four seconds. In the last three seconds, the frequency and amplitude changed to 1 Hz and 30 degrees. The predefined excitation trajectory can be shown as

$$\theta_d = \begin{cases} 45\sin(0.5\pi t) & \text{deg} \quad 0 \le t < 8\ \text{s} \\ 60\sin(\pi(t-8)) & \text{deg} \quad 8 \le t < 12\ \text{s} \\ 30\sin(2\pi(t-12)) & \text{deg} \quad 12 \le t < 15\ \text{s} \end{cases} \tag{21}$$

Fig. 7. Upper-limb rehabilitation exoskeleton and subject in test

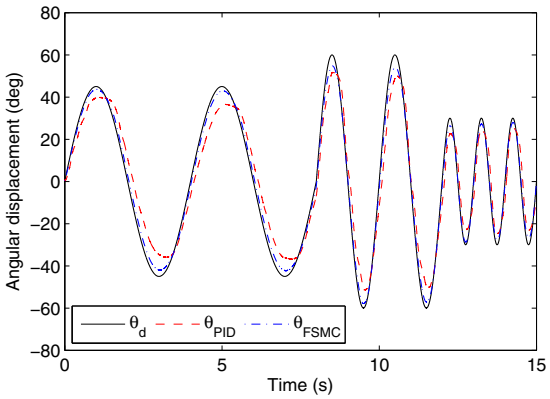

Fig. 8. Results of the sinusoid trajectory tracking experiments using PID algorithm and fuzzy SMC algorithm

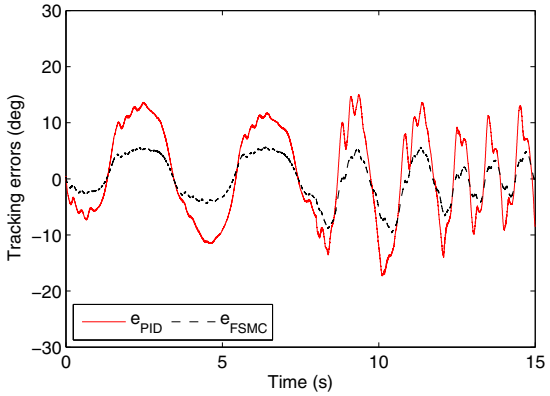

Fig. 9. Comparison of the tracking errors for the different algorithms

The sinusoid trajectory tracking results are demonstrated in Fig. 8 and Fig. 9. As can be observed, the tracking performance of the fuzzy SMC algorithm goes better than that of the conventional PID controller. More specifically, the average position tracking errors decline from 11.42% (PID controller) to 4.15% (fuzzy SMC algorithm) during the experiments. Besides, it should be noticed that the undesirable chattering phenomenon caused by the hitting term control law has been significantly reduced by using the nonlinear fuzzy algorithm. The results confirm the validity of the proposed strategy for position control.

V. Conclusion and Future Works

This paper has introduced and described a therapeutic exoskeleton device for the upper-limb rehabilitation of the patients with motor dysfunction. The mechanical structure of the robotic system is kinematically similar to human arm anatomy, enabling natural interaction with the user. A Matlab/RTW-based control system is established for the real-time control of the exoskeleton. A novel SMC algorithm with a PID sliding surface and a fuzzy turning hitting control law has been developed to eliminate the chattering problem and improve the performance of the therapy training. The stability of the proposed control strategy is mathematically demonstrated via the Lyapunov theorem. Further sinusoid trajectory tracking experiments are conducted with a volunteer to prove the effectiveness of the fuzzy SMC algorithm. The experimental results that are compared to the conventional PID controller indicate that the average tracking errors of the proposed control strategy have been effectively reduced. Future works will be devoted to develop the active control algorithm for the patient-cooperative therapy, which is capable of estimating the motion intention of user and applying desired active support during rehabilitation training.

Acknowledgment

This research has been supported by the Fundamental Research Funds for the Central Universities (CXZZ13_0085), the Scientific Research Foundation of Graduate School of Southeast University (YBJJ1427), and the China Nation Nature Science Foundation under grant 51175078.

References

[1] A. Picelli, S. Tamburin, M. Passuello, A, Waldner, and N, Smania, “Robot-assisted arm training in patients with Parkinson’s disease: a pilot study,” Journal of neuroengineering and rehabilitation, vol. 11, no. 1, pp. 1–4, 2014.

[2] A. Timmermans, R. Lemmens, M. Monfrance, R. Geers, W. Bakx, R. Smeets, et al, “Effects of task-oriented robot training on arm function, activity, and quality of life in chronic stroke patients: a randomized controlled trial,” Journal of neuroengineering and rehabilitation, vol. 11, no. 45, pp. 1–11, 2014.

[3] Q. C. Wu, X. S. Wang, and F. P. Du, “Development and control of a bowden-cable actuated exoskeleton for upper-limb rehabilitation,” IEEE International Symposium on Robotic and Sensors Environments, pp. 7–12, 2014.

[4] Z, Tang, K. Zhang, S. Sun, Z. Gao, L. Zhang, and Z. Yang, “An upper-limb power-assist exoskeleton using proportional myoelectric control,” Sensors, vol. 14, no. 4, pp. 6677–6694, 2014.

[5] V. Klamroth, J. Blanco, K. Campen, A. Curt, V. Dietz, T. Ettlin, et al, “Three-dimensional, task-specific robot therapy of the arm after stroke: a multicentre, parallel-group randomised trial”, The Lancet Neurology, vol. 13, no. 2, pp. 159–166, 2014.

[6] M. S. Ju, C. C. Lin, D. H. Lin, I. Hwang, and S. M. Chen, “A rehabilitation robot with force-position hybrid fuzzy controller: hybrid fuzzy control of rehabilitation robot,” IEEE Transactions on Neural Systems and Rehabilitation Engineering, vol. 13, no. 3, pp. 349-358, 2005.

[7] T. Nef, M. Mihelj, G. Kiefer, C. Perndl, R. Muller, and R. Riener, “ARMin-exoskeleton for arm therapy in stroke patients,” IEEE 10th International Conference on Rehabilitation Robotics, PP. 68–74, 2007.

[8] X. Z. Jiang, X. H. Huang, C. H. Xiong, R. L. Sun, and Y. L. Xiong, “Position control of a rehabilitation robotic joint based on neuron proportion-integral and feedforward control,” Journal of Computational and Nonlinear Dynamics, vol. 7, no. 2, 2012.

[9] W. Yu, J. Rosen, and X. Li, “PID admittance control for an upper limb exoskeleton,” IEEE American Control Conference, pp. 1124–1129,2011.

[10] A. F. Amer, E. A. Sallam, and W. M. Elawady, “Adaptive fuzzy sliding mode control using supervisory fuzzy control for 3 DOF planar robot manipulators,” Applied Soft Computing, vol. 11, no. 8, pp. 4943-4953, 2011.

[11] F. G. Rossomando, C. Soria, and R. Carelli, “Sliding mode neuro adaptive control in trajectory tracking for mobile robots,” Journal of Intelligent & Robotic Systems, vol. 74, no. 3, pp. 931–944, 2014.

[12] O. Barambones, and P. Alkorta, “Position control of the induction motor using an adaptive sliding mode controller and observers,” IEEE Transactions on Industrial Electronics, vol. 61, no. 12, pp. 6556-6565, 2014.

[13] A. Denève, S. Moughamir, and L. Afilal, “Control system design of a 3-DOF upper limbs rehabilitation robot,” Computer methods and programs in biomedicine, vol. 89, no. 2, pp. 202–214, 2008.

[14] N. T. Tai, and K. K. Ahn, “A RBF neural network sliding mode controller for SMA actuator,” International Journal of Control, Automation and Systems, vol. 8, no. 6, pp. 1296-1305, 2010.

[15] H. Aschemann, and D. Schindele, “Sliding-mode control of a high-speed linear axis driven by pneumatic muscle actuators,” IEEE Transactions on Industrial Electronics, vol. 55, no.11, pp. 3855–3864, 2008.

[16] K. Erbatur, and O. Kaynak, “Use of adaptive fuzzy systems in parameter tuning of sliding-mode controllers,” IEEE/ASME Transactions on Mechatronics, vol.6, no.4, pp. 474–482, 2011.

[17] M. Rahman, M. Saad, and J. P. Kenné, “Control of an exoskeleton robot arm with sliding mode exponential reaching law,” International Journal of Control, Automation and Systems, vol.11, no.1, pp. 92–104, 2013.

[18] G. Bartolini, A. Ferrara, and E. Usani, “Chattering avoidance by second-order sliding mode control,” IEEE Transactions on Automatic control, vol. 43, no.2, pp. 241-246, 1998.

[19] Q. C. Wu, and X. S. Wang, “Design of a gravity balanced upper limb exoskeleton with bowden cable actuators,” 2013 IFAC Symposium on Mechatronic Systems, pp. 679–683, 2013.

[20] Q. C. Wu, X. S. Wang, L. Chen, and F. P. Du, “Transmission model and compensation control of double-tendon-sheath actuation system,” IEEE Transactions on Industrial Electronics, vol. 62, no. 3, pp. 1599–1609, 2015.

[21] Q. C. Wu, X. S. Wang, F. P. Du, and X. B. Zhang, “Design and Control of a Powered Hip Exoskeleton for Walking Assistance,” International Journal of Advanced Robotic Systems, vol. 12, no. 18, pp. 1-11, 2015.

[22] C. J. Fallaha, M. Saad, H. Y. Kanaan, and K. Haddad, “Sliding-mode robot control with exponential reaching law,” IEEE Transactions on Industrial Electronics, vol. 58, no. 2, pp. 600–610, 2011.

[23] T. Orowska, M. Kaminski, and K. Szabat, “Implementation of a sliding-mode controller with an integral function and fuzzy gain value for the electrical drive with an elastic joint,” IEEE Transactions on Industrial Electronics, vol. 57, no. 4, pp. 1309–1317, 2010.

[24] D. Winter, Biomechanics and motor control of human movement, 4th ed, Ontario: Waterloo, 2004, pp. 86–87.

[25] J. G. Ziegler, and N. B. Nichols, “Optimum settings for automatic controllers,” Transactions of the ASME, Vol. 64, pp. 759–768, 1942.